

# High-Temperature Oxidation Behaviour of CrSi Coatings on 316 Austenitic Stainless Steel

Gurtaran, Mikdat; Zhang, Zhenxue; Li, Xiaoying; Dong, Hanshan

DOI:

[10.3390/ma16093533](https://doi.org/10.3390/ma16093533)

License:

Creative Commons: Attribution (CC BY)

*Document Version*

Publisher's PDF, also known as Version of record

*Citation for published version (Harvard):*

Gurtaran, M, Zhang, Z, Li, X & Dong, H 2023, 'High-Temperature Oxidation Behaviour of CrSi Coatings on 316 Austenitic Stainless Steel', *Materials*, vol. 16, no. 9, 3533. <https://doi.org/10.3390/ma16093533>

[Link to publication on Research at Birmingham portal](#)

## General rights

Unless a licence is specified above, all rights (including copyright and moral rights) in this document are retained by the authors and/or the copyright holders. The express permission of the copyright holder must be obtained for any use of this material other than for purposes permitted by law.

- Users may freely distribute the URL that is used to identify this publication.
- Users may download and/or print one copy of the publication from the University of Birmingham research portal for the purpose of private study or non-commercial research.
- User may use extracts from the document in line with the concept of 'fair dealing' under the Copyright, Designs and Patents Act 1988 (?)
- Users may not further distribute the material nor use it for the purposes of commercial gain.

Where a licence is displayed above, please note the terms and conditions of the licence govern your use of this document.

When citing, please reference the published version.

## Take down policy

While the University of Birmingham exercises care and attention in making items available there are rare occasions when an item has been uploaded in error or has been deemed to be commercially or otherwise sensitive.

If you believe that this is the case for this document, please contact [UBIRA@lists.bham.ac.uk](mailto:UBIRA@lists.bham.ac.uk) providing details and we will remove access to the work immediately and investigate.

## Article

# High-Temperature Oxidation Behaviour of CrSi Coatings on 316 Austenitic Stainless Steel

Mikdat Gurtaran <sup>\*</sup>, Zhenxue Zhang , Xiaoying Li  and Hanshan Dong 

School of Metallurgy and Materials, The University of Birmingham, Birmingham B15 2TT, UK

<sup>\*</sup> Correspondence: m.gurtaran@bham.ac.uk

**Abstract:** In this study, a closed-field unbalanced magnetron sputtering system, which is environmentally friendly and has high deposition efficiency, was used to deposit CrSi coatings on 316 austenitic stainless steel. This system utilised separate Cr and Si targets, and the appropriate content of Cr and Si of the coatings was adjusted by changing the currents applied to the targets. A series of CrSi coatings with different Si/Cr ratios were produced, and their oxidation behaviour at elevated temperatures was investigated. By analysing the weight gain, surface morphology and microstructure, composition and phase constituents, the oxidation behaviour at 600 °C, 700 °C and 800 °C was investigated and the optimized coating to protect the stainless steel has been identified. The outcome of the research indicated that a small amount of Si (between 4–7 at.%) in Cr coatings is effective in protecting the austenitic stainless steel against oxidation at high temperatures, while a high Si content (around 10 at.% or more) makes the coating more brittle and prone to cracking or delamination during oxidation at 800 °C.

**Keywords:** CrSi coatings; magnetron sputtering; oxidation; 316 stainless steel



**Citation:** Gurtaran, M.; Zhang, Z.; Li, X.; Dong, H. High-Temperature Oxidation Behaviour of CrSi Coatings on 316 Austenitic Stainless Steel. *Materials* **2023**, *16*, 3533. <https://doi.org/10.3390/ma16093533>

Academic Editor: Carlos Garcia-Mateo

Received: 29 March 2023

Revised: 27 April 2023

Accepted: 3 May 2023

Published: 5 May 2023



**Copyright:** © 2023 by the authors. Licensee MDPI, Basel, Switzerland. This article is an open access article distributed under the terms and conditions of the Creative Commons Attribution (CC BY) license (<https://creativecommons.org/licenses/by/4.0/>).

## 1. Introduction

Austenitic stainless steels are materials of choice for many engineering applications, ranging from nuclear power stations to the chemical industry [1–4], mainly due to their excellent mechanical properties and high corrosion resistance [5,6]. However, the oxidation resistance of austenitic stainless steels needs to be better for such high-temperature applications as rocket engines [7] or the petrochemical industry [8]. In addition, in many high-temperature applications, large temperature change leads to oxide layer spallation because of the thermal expansion differences between the oxide layer formed on the surface and the austenitic stainless steel substrate. Consequently, rapid oxidation of the austenitic stainless steel occurs when it is exposed to an aggressive environment without a protective oxide layer. To extend their service life, the areas of the material in contact with the aggressive environment are made resistant by applying different protective coatings [9,10].

There are many scientific studies on ceramic or metal-based protective coatings applied to stainless steel using different techniques [11–14]. Metals such as Al, Cr, Ti, and Si are frequently used in protective coatings as their oxides have considerably high oxidation resistance at high temperatures [15–17]. Different coatings are applied to increase oxidation resistance at medium and high temperatures [18–20]. However, new coatings with desirable oxidation behaviour at high temperatures need to be developed to address the limitations of currently available coatings.

Recently, Cr has drawn increasing attention due to its good antioxidant effect at high temperatures [21–24]. Characteristically, chromium exhibits good oxidation resistance at high temperatures, with very few crystalline defects that cause an increase in oxidation kinetics [25,26]. However, its use in high-temperature applications is limited due to insufficient mechanical properties causing physical cracking and breakage [27]. In addition, pure Cr coating is completely oxidised at high temperatures [25,28] and does not provide

effective oxidation protection unless it has a thickness of more than 11  $\mu\text{m}$  [29,30]. Hence, it has been suggested that a small amount of Si in Cr coatings may improve the oxidation resistance due to the reduction in the oxidation kinetics owing to the single-phase solid solution formed by Si atoms in the CrSi structure [31–33]. CrSi coatings have been studied to protect zircaloy 4 [31–34], Ti-46Al-8N [35], and zirconium-based materials [36] against oxidation at high temperatures.

In the last decade, the production of Cr-based coatings using Cr plating baths has been dramatically reduced and almost fully restricted in Europe due to the formation of toxic chromic acid (known as hexavalent chromium) [37], which is quite hazardous for human health [38]. In this study, a closed-field unbalanced magnetron sputtering system, which is environmentally friendly, was used to deposit CrSi coatings on 316 austenitic stainless steel with a high deposition efficiency. Generally, it is reported in the literature that a CrSi target with a constant Cr and Si composition is used to generate the CrSi coating with fixed composition [27,35,36]. In this study, the closed-field unbalanced magnetron sputtering system utilises separate Cr and Si targets so that the appropriate content of Cr and Si in the coating can be easily adjusted by applying different currents on the targets. In this research, a series of CrSi coatings with different amounts of silicon were produced and their oxidation behaviour at 600–800 °C was investigated. By analysing the weight gain, observing coating morphology and microstructure and studying the composition and phase constituents, the oxidation behaviour of the CrSi coatings was fully studied and the optimised coating used to protect the stainless steel was identified. Application of the CrSi coatings on thermoelectric materials for oxidation resistance will be carried out and the current study will provide solid background knowledge for further investigation.

## 2. Experimental

### 2.1. Sample Preparation and CrSi Coating Processes

A commercial austenitic stainless-steel rod (Goodfellow, Huntingdon, UK) with a diameter of 25.4 mm was cut (using Struers Accutom-50) to specimens with a thickness of 5 mm. The elemental constituents of the as-received austenitic stainless steel are presented in Table 1. The samples were ground using SiC abrasive papers up to 1200 grit. Before the coating process, the samples were ultrasonically cleaned in acetone and deionised water for 10 min.

**Table 1.** The chemical composition (at.%) of AISI 316 stainless steel used in this study.

Elements	Carbon	Silicon	Manganese	Chromium	Nickel	Molybdenum	Iron	Other
AISI 316	0.03	1.00	2.00	16.50–18.50	10.00–13.00	2.00–2.50	Bal.	<1.00

CrSi coatings with different compositions were applied to the austenitic stainless steel substrate using the closed-field unbalanced magnetron sputtering technique (Teer Coatings Ltd., Droitwich, UK). Cr and Si targets were placed opposite each other into the physical vapour deposition (PVD) equipment. A constant current of 2 A was applied to the Cr cathode target, while the currents of 0.2, 0.3, and 0.4 A were applied to the Si cathode target to adjust the Si composition in the coatings deposited. The rotation speed of the sample was 5 rpm. The coating process was carried out in three steps: (1) 15 min of ion cleaning of the sample surface using a low current of 0.05 A and 0.2 A for Si and Cr targets under a bias potential of 200 V to remove any contamination; (2) the current of target Cr and Si was ramped up to 0.3/0.4/0.5 A and 2 A in 4-min, and the bias potential was reduced gradually from 200 V to 40 V; (3) deposition of CrSi coating for 35 min at a pressure of  $13.33 \times 10^{-2}$  Pa within the argon atmosphere. Due to the ion bombardment, the sample temperature increased slightly in the deposition process to about 100 °C.

## 2.2. Oxidation Testing

A few CrSi-coated samples were oxidised in the air at 600 °C, 700 °C, and 800 °C, respectively, for 80 h, which represented typical operating conditions for many high-temperature applications, using a muffle furnace (SNOL-TMS Europe Ltd., Bradwell, UK) and cooled rapidly (about 50 °C/min) to room temperature in the air environment. Repeated oxidation was taken for the CS4-O8 samples and similar outcomes were confirmed. The weights of the samples were measured using the Ohaus sensitive scale with a sensitivity of  $10^{-4}$  g before and after the oxidation testing.

## 2.3. Microstructure Characterization and Property Evaluation

Systematic microstructure characterisation was performed on both CrSi-coated and oxidised CrSi-coated samples. Surface morphologies and cross-sectional microstructure were investigated using scanning electron microscopy (SEM, Jeol 7000, and Apreo 2 (Jeol-UK Ltd., Welwyn Garden City, UK and Thermofisher Scientific, Stafford, UK), respectively) with EDX devices for chemical concentration and distribution analysis. The surface roughness was also measured using an Ambious XP-200 profilometer (Cnitech, Wisbech, UK) with a scanning speed of 0.05 mm/s, over 8 mm length. Proto AXRD diffractometer with a Cu-K $\alpha$  source ( $\lambda = 1.540598 \text{ \AA}$ ) was used to identify the phases of the CrSi coatings. The codes of the samples and corresponding processing parameters are detailed in Table 2. Sample codes of SS, SS-O6, SS-O7, and SS-O8 were given to related stainless steel and oxidised stainless steel samples at 600 °C, 700 °C, and 800 °C, respectively.

**Table 2.** Codes of the samples and corresponding process parameters.

Coating Parameters (Currents)	Sample Codes for CrSi Coatings	Sample Codes for Oxidised Coating Samples		
		600 °C—80 h (O6)	700 °C—80 h (O7)	800 °C—80 h (O8)
Cr (2 A) Si (0.2 A)	CS2	CS2-O6	CS2-O7	CS2-O8
Cr (2 A) Si (0.3 A)	CS3	CS3-O6	CS3-O7	CS3-O8
Cr (2 A) Si (0.4 A)	CS4	CS4-O6	CS4-O7	CS4-O8

## 3. Results

### 3.1. Microstructure of CrSi Coatings

As shown in Figure 1, the coatings deposited are dense and uniform on the 316 substrates with a fine columnar structure, and the diameter of the column is inversely related to the current applied to the Si target during the coating processes. No pores and spallation were observed on the surface of the coatings. The thickness of the coating layers was around 1.5  $\mu\text{m}$ . EDX analysis of the three CrSi coatings revealed that the atomic composition of Si content increased from 4.32% to 7.16% and 9.39%, corresponding to the Si target current of 0.2 A, 0.3 A, and 0.4 A, respectively, accompanied by the decrease in the column diameter. It implies that the high Si content facilitated the nucleation of the columns. The surface roughness was almost identical for all the coatings,  $R_a = 0.15 \pm 0.010 \text{ (\mu m)}$ , confirming the uniform coating structures observed by SEM.

XRD patterns taken from CrSi coating samples are presented in Figure 2, compared with the pattern of the substrate 316 sample. It can be seen that the substrate phase of austenitic stainless steel was detected from all three coating samples, as indicated at  $2\theta$  of  $43.8^\circ$  and  $51^\circ$  for (111) and (200) planes. No crystallographic reflection corresponding to the CrSi phases was detected from the coating samples, but still, a dominant (110) signal of reflection corresponding to the Cr-body-centred cubic (bcc) phase was identified, indicating the preferred orientation of the columnar structure with a (110) perpendicular to the surface.

It was observed that the position of the (110) signal of reflection with higher Si content was shifted towards a higher angle, and this is due to the decrease in the lattice constant caused by the Si atom in the form of a solid solution. When the Si content reached 9.39 at% (CS4 sample), the intensity of the (110) reduced with a larger full width at half maximum (FWHM), which indicates a distorted crystal structure of Cr and also reduced the preferred columnar growing direction of [110].

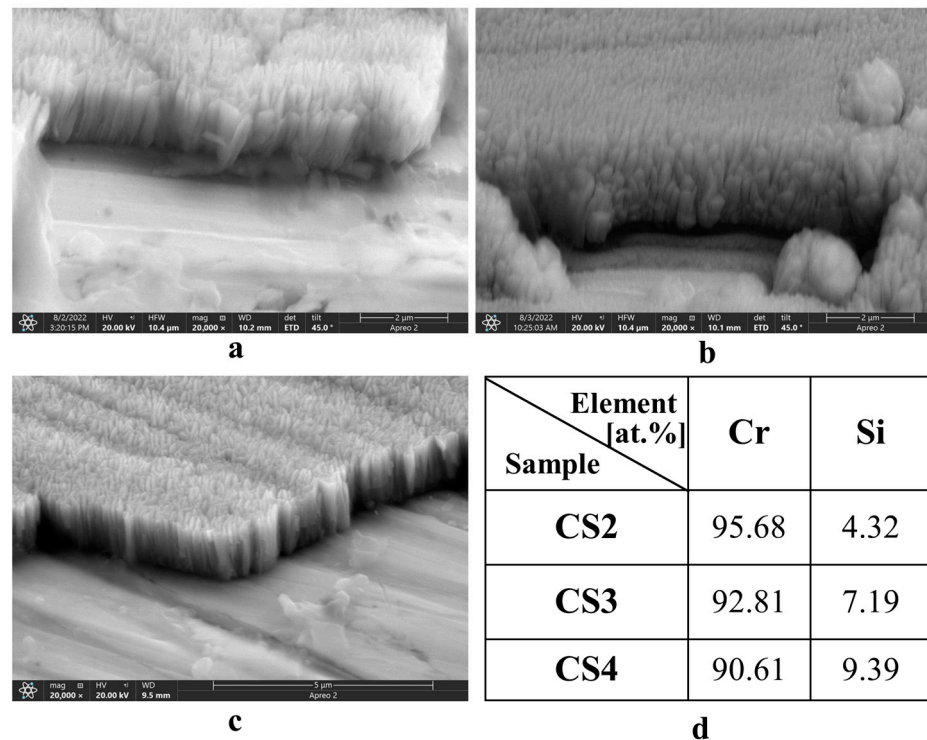


Figure 1. Cross-sectional SEM images of CrSi coating samples (a) CS2, (b) CS3, (c) CS4, and (d) EDX analysis of elemental composition (atomic%) for CrSi coating samples.

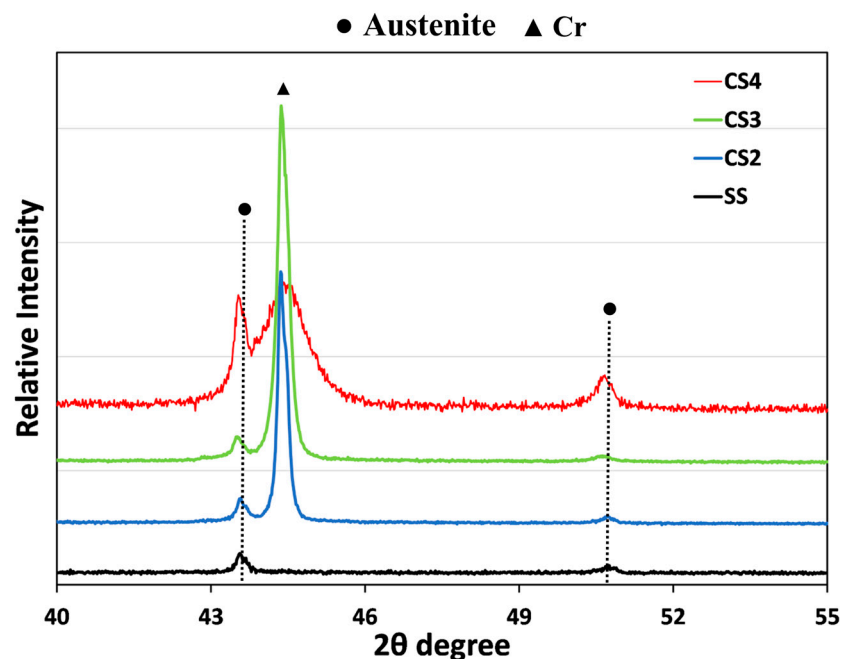
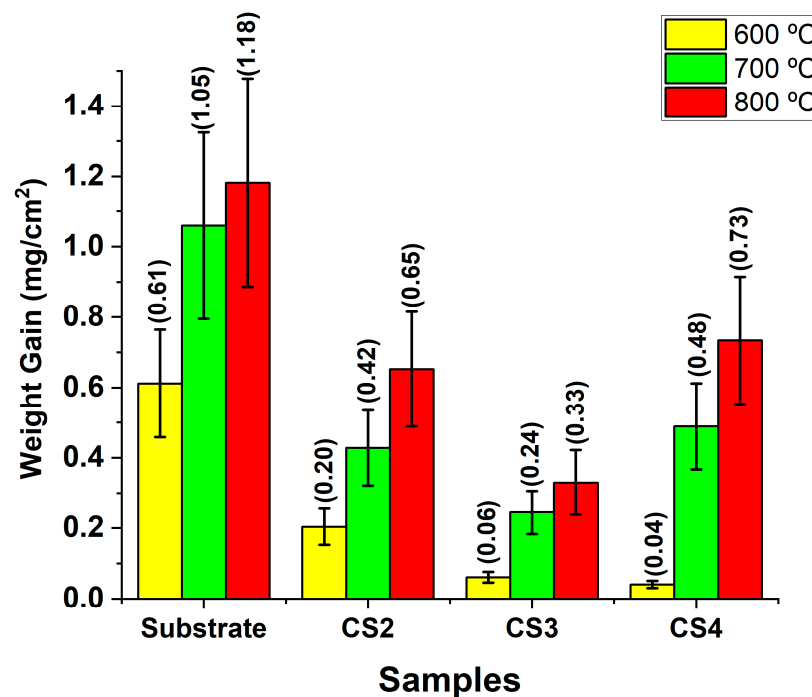


Figure 2. XRD patterns of CrSi coating samples (PDF: 01-085-1335) and AISI316 matrix sample (SS) (PDF: 00-003-1209).

### 3.2. Oxidation Behaviour

#### 3.2.1. Weight Gain and Surface Morphology

Weight gain of stainless steel and CrSi coated samples after oxidation testing at 600 °C, 700 °C, and 800 °C was given in Figure 3. It can be seen that generally, the weight gain changes proportionally to the oxidation temperatures. However, all three CrSi coatings showed a significant reduction in weight gain as compared with the 316 substrate. It can also be seen that the least oxidation weight gain, 0.04 mg/cm<sup>2</sup>, was observed for the CS4-O6 coating sample. When the oxidation temperature was above 700 °C, CS3 coating samples performed the best among all the coating samples with a lower weight gain of 0.24 and 0.33 mg/cm<sup>2</sup> for 700 °C and 800 °C, respectively.



**Figure 3.** Weight gain of the oxidised CrSi coating samples with the oxidised stainless steel substrate (SS) as a comparison.

SEM observation on the surface of oxidised samples revealed similar morphology for the samples oxidised at the same temperatures regardless of the Si contents, and the typical SEM images are shown in Figure 4. It can be seen that after oxidation at a temperature above 600 °C, irregular polygonal oxide particles formed on the surface of the coatings and the higher the temperature, the larger the particles (Figure 4b,c). Some partial spallation was observed for 800 °C oxidised coating samples. However, most of the surface area was still protected by the CrSi coatings (Figure 4e). In contrast, the surface of 316 steel was severely damaged after exposure to 800 °C, as shown in Figure 4f.

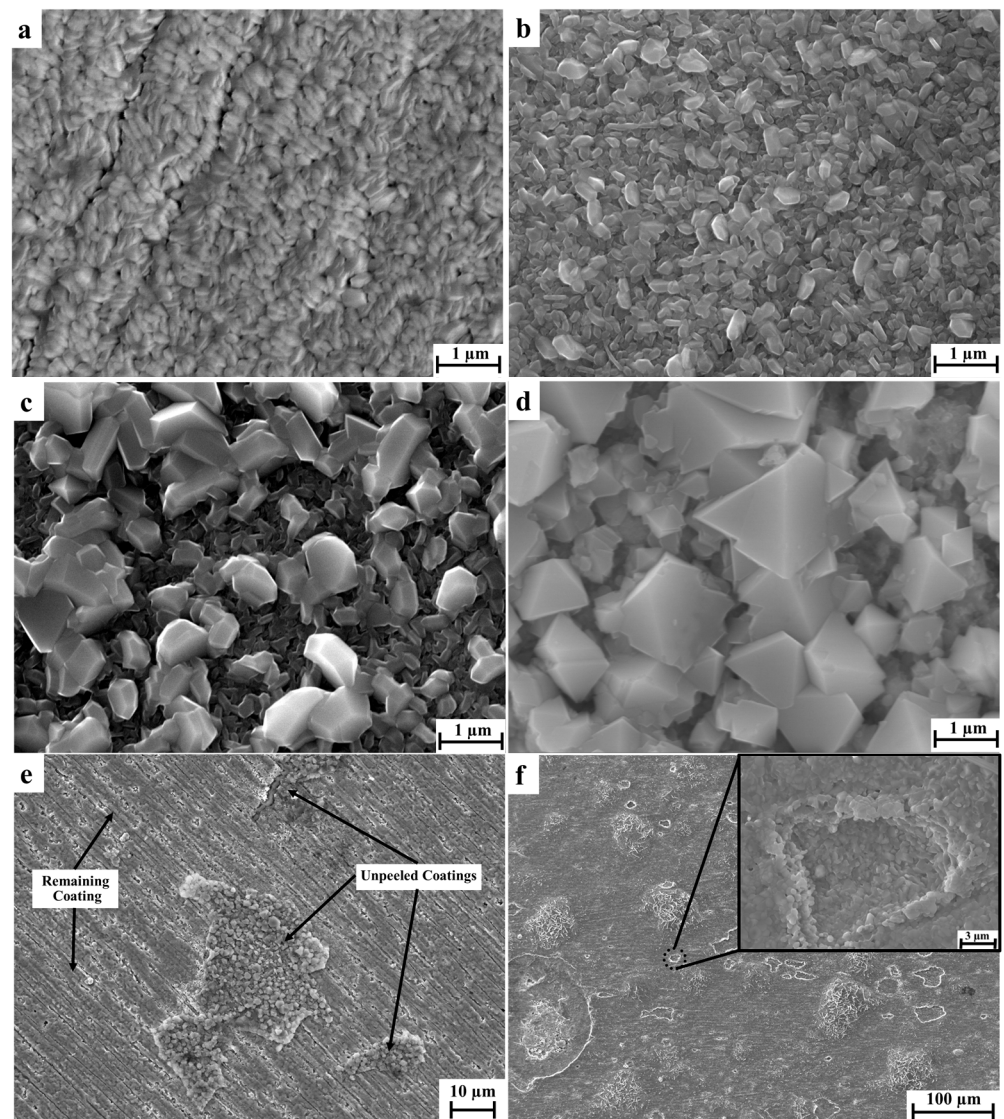


**Figure 4.** Typical surface morphologies of (a) CS3, (b) CS3-O6, (c) CS3-O7, (d) CS4-O8 (high magnification), (e) CS4-O8 (low magnification), (f) SS-O8.

### 3.2.2. Oxide Layer Structure

XRD patterns of the coating samples indicate identical crystallographic reflections when oxidised at the same temperature regardless of the Si content variations. Figure 5 presented typical XRD patterns of the coating samples oxidised at different temperatures compared with XRD patterns of 316 steel and SS-O8 samples. It can be observed that Cr (110) was detected for all oxidised samples, with the intensity of it inversely related to the oxidation temperatures (Figure 5a). A few chromium oxide phases were identified from the CS2-O6 sample. For 700 °C and 800 °C oxidised CS samples, more crystallographic reflections corresponding to chromium and silicide oxides were detected. No signal of reflections of ferrous oxides was detected from all coating samples, indicating oxidation protection of CrSi coatings on the stainless steel surface. The XRD pattern of the 800 °C oxidised stainless steel sample reveals strong  $(\text{FeCr})_3\text{O}_4$  and  $\text{Fe}_2\text{O}_3$  crystallographic reflections, and the matrix phase of austenitic stainless steel is hard to identify, which implies a thick oxide layer formation on the surface. XRD patterns of different Si content CrSi coating samples after 800 °C oxidation treatment are shown in Figure 5b, with SS-O8 as a comparison. It can be seen that strong intensity and more reflections of the  $\text{Cr}_2\text{O}_3$  and  $\text{SiO}_2$  phases were detected for samples with a higher Si content.

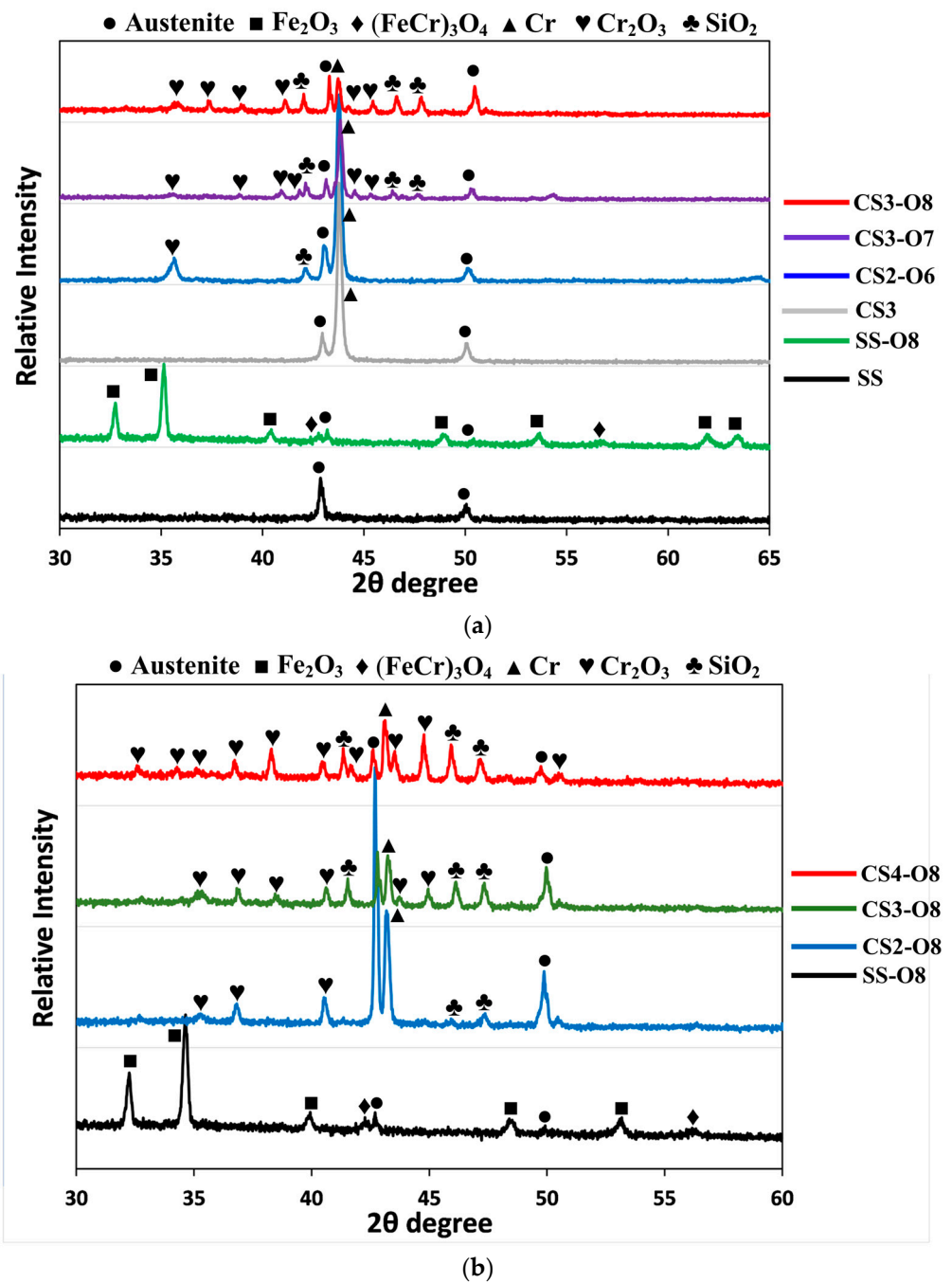


**Figure 5.** Typical XRD patterns of (a) oxidised CrSi coating samples compared with CrSi coating sample, substrate stainless steel and 800 °C oxidised stainless steel sample; and (b) 800 °C oxidation treated CrSi samples with different Si content compared with the stainless steel treated at the same condition (PDFs: 00-003-1175, 01-076-1821, 01-076-0938, 01-084-0313).

SEM observation and EDX elements mapping analysis on cross-sectionally prepared oxide layer samples revealed elements distributed evenly within the CrSi coating layer. A typical SEM image, overlaid with EDX maps of Si, Cr, Fe, and O for sample CS4-O8 is shown in Figure 6. It is indicated that neither Si nor Cr were segregated within the coating layer even after 800 °C oxidation.



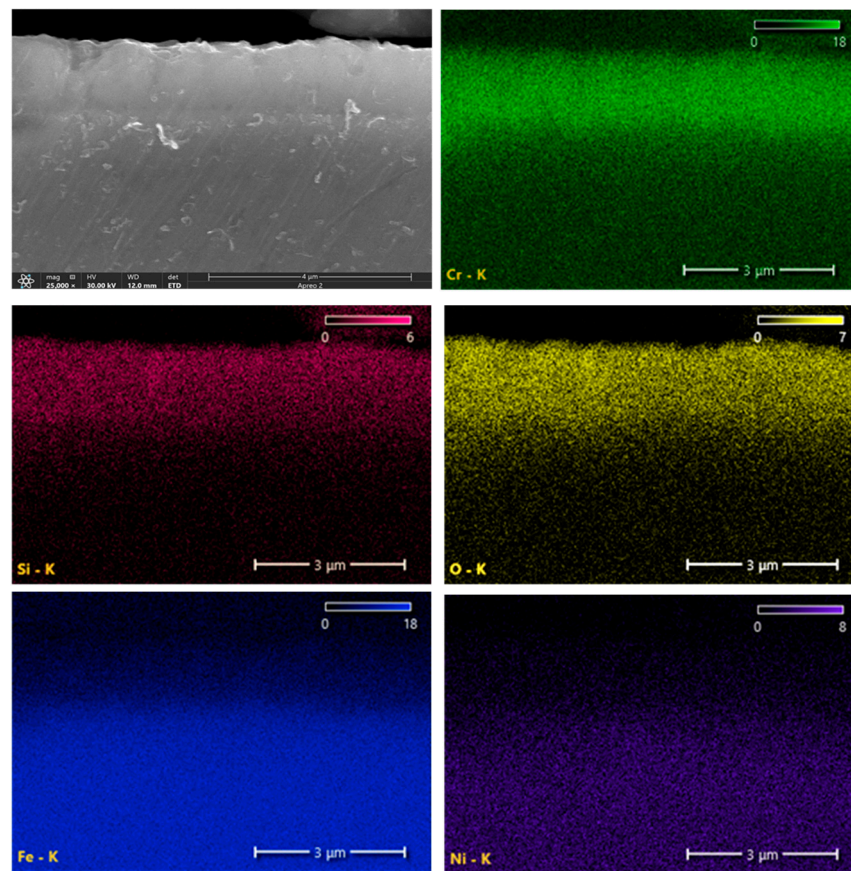


**Figure 6.** Cross-sectional SEM image of sample CS4-O8 with EDX count-mapping showing elements distributed evenly within the CrSi coating layer.

Colour Chemi SEM observation on fractured oxidation-treated samples revealed the layer structure differences between the coatings with Si contents. As shown in Figure 7, a thin surface oxide layer formed on CS-O6 samples, and the layer thickness is thicker for lower Si content samples than for the higher ones. Underneath the oxide layer, the CrSi coating layer still adhered to the substrate firmly; no spallation and cracks were found. For 700 °C oxidised CrSi coating samples, the top surface formed a thicker oxide layer, and a few patches of top oxides layer peeling off were observed. However, most formed oxide films protected the austenitic stainless steel surface against oxidation. In particular, the CS3-O7 sample performed less oxidation, as evidenced in Figure 7, where a thick CrSi layer remained on the substrate. However, CrSi coating samples were peeled off of the formed thin surface oxides layer when oxidised at 800 °C; the severity of this phenomenon is related to the Si content of the coatings. For CS2 and CS3 samples, the peeling only happened on the top surface of the formed oxide film, and the CrSi coating layer remained after 80 h oxidation and protected the stainless steel surface from oxidation. However, for sample CS4, which had a coating with a high Si content, not only was the superficial oxide layer that formed on the surface peeled off, but the whole coating layer in some areas was also removed, indicating weak adhesion between the coating and the substrate after 800 °C/80 h oxidation testing when the Si content reached about 10 at.%.

It has also been observed that the oxides formed at 800 °C featured differently as a function of the Si content of the coatings. For low-content Si CS2 samples, the formed oxides are in the shape of round particles of 500 nm in diameter, whereas for medium Si-content CS3 samples, triangular-faceted grains with a diameter of 1200 nm were formed. Further increasing the Si content to about 10 at.%, the formed oxides are mixed with thin rods and round particles in the size of 1700 nm (Figure 7).

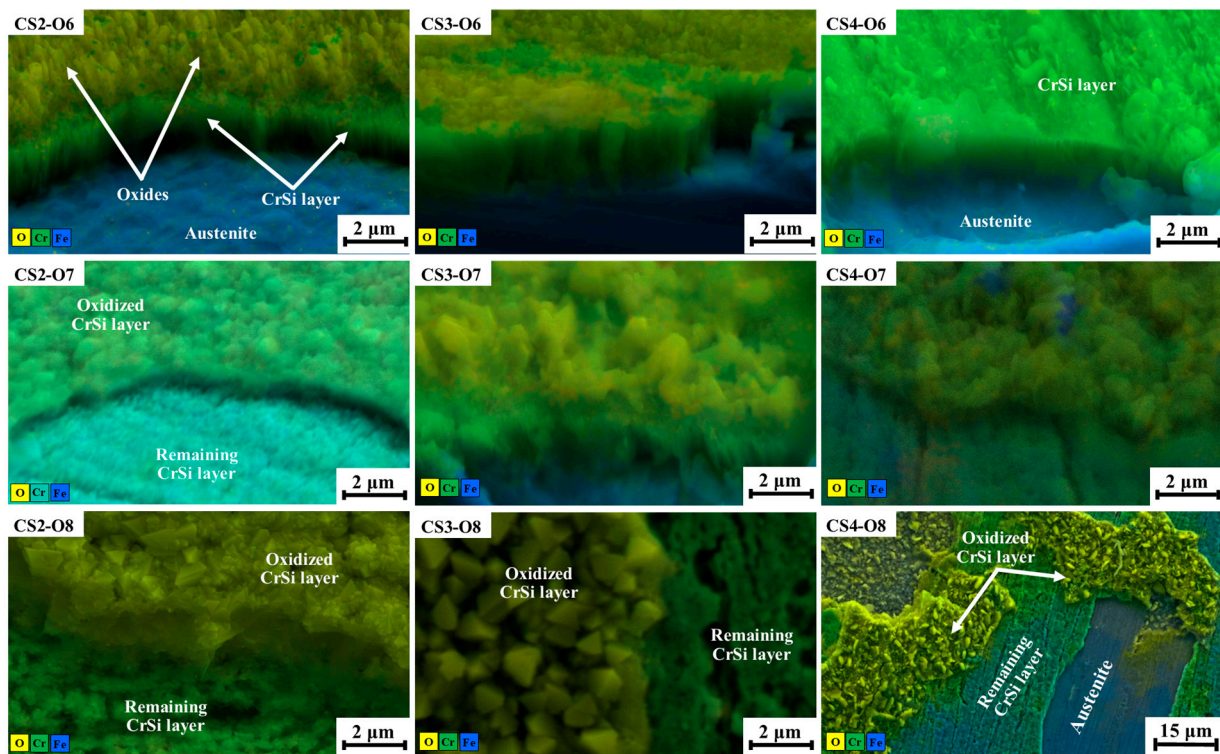


Figure 7. Colour chemi SEM images of fractured oxidised CrSi coating samples as indicated.

#### 4. Discussion

A series of CrSi-based coatings with varying Si contents have been observed to withstand damage upon oxidation at high temperatures. As shown in Figure 3, after the oxidation testing, all the CrSi coated samples revealed less weight gain than the stainless steel substrate, which indicates that the CrSi coatings could protect the 316 stainless steel substrate from oxidation. Compared with the oxidation behaviour of the coating samples with different levels of Si concentration, it can be seen from Figure 3 that CS3 and CS4 coatings performed better than CS2 at an oxidation temperature of 600 °C, while CS3 is superior to that CS2 and CS4 coating samples with the lowest weight gain when oxidised at temperatures of 700 °C and 800 °C. The results demonstrate that the extent of the oxidation resistance is Si/Cr ratio related. XRD patterns of the CrSi coatings (Figure 5) confirm that the main phase of the three CrSi coatings (4.3–9.4 at.% Si) is the Cr phase with a body-centred cubic structure. With increasing Si content, the (110) reflection became broader and shifted more to a higher 2 theta angle, or reduced d-spacing of (110), due to the existence of Si atoms in Cr lattices where Si with a smaller radius to replace Cr when in the solid solution. This is in line with the fact that the solubility of Si in Cr is at an atomic concentration between 4.3 and 9.4 (at.%) [39]. The decreased lattice constant will induce crystal structure distortion, making the Cr atoms much more difficult to move and delaying chromium oxide formation.

The hypothesis under consideration is substantiated by the SEM images presented in Figure 7, which depict the elemental distribution of oxidised CrSi-coated samples. The revealed thickness of the top surface oxide layer reduces with increasing Si content, except for CS4, when oxidised at 700 °C and 800 °C. This exception may be related to the coating microstructure of CS4. As revealed in Figure 1, the columnar structure of CS4 is much thinner than CS2 and CS3, implying dense columnar boundaries of CS4, which would be the oxygen diffusion tunnels. It is well known that the oxygen diffusion coefficient along grain boundary is 108 times greater than that of bulk diffusion [40]. This is due to the atomic jump frequency in these planar defects, which is about a million times greater than the jump frequency of regular lattice atoms [41]. This fast diffusion of oxygen at high

temperatures along columnar boundaries resulted in the worse oxidation resistance of CS4 coating samples. Consequently, oxygen could diffuse to the interface along some loose boundaries and meet with the substrate to form iron oxide, which weakens the adhesion of the CrSi coating to the substrate. This hypothesis was supported by the fact that CS4 coating peeled off more from the substrate than CS2 and CS3 coating samples when oxidised at 800 °C for 80 h (Figure 7). Furthermore, as depicted in Figure 3, the hypothesis under consideration may serve as a probable explanation for the observed weight gain in the CS4-O8 sample. These outcomes are in line with the literature. Zeng, Song et al. [34] suggested that 8% (at.) of Si content in CrSi coatings provides the optimum performance against oxidation at 1200 °C. Similar outcomes were also found by He, Xiujie et al. [36], who stated the superior oxidation behaviour of CrSi coatings with relatively low Si content at high temperatures. Based on the previous studies in the literature and our findings, a further investigation, including oxidation kinetics will be carried out in a follow-up study to see the protectivity of the scale against oxidation.

## 5. Conclusions

CrSi coatings with different Si concentrations ranging from 4.32 to 9.39 at.% were deposited on 316 stainless-steel substrates using a closed-field unbalanced magnetron sputtering technique. The thickness of all three CrSi coatings is about 1.5 µm and the coating layers are compact with a columnar structure, but the column diameter decreased with increasing the Si concentration.

The oxidation behaviour of the fabricated CrSi coatings at 600 °C, 700 °C, and 800 °C was investigated. Generally, all the coatings possessed good oxidation resistance to protect the 316 stainless steel substrate, and the higher the Si content, the better the oxidation resistance when tested at 600 °C. A superficial oxide layer on the surface of the CrSi coating can prevent further oxidation, thus protecting the stainless steel surfaces from oxidation. A medium amount of Si (7–8 at.%) in the chromium coating (CS3) demonstrated the best oxidation protection of the stainless steel samples when tested at 700 °C and 800 °C. The relatively poorer oxidation protection performance of the CS4 coating, with a high silicon content of 9.4 at.%, is related to the fine columnar structure, which led to fast diffusion of oxygen to the interface between the coating and the substrate, forming iron oxide and thus causing spallation of the coating layer.

Based on these findings, it can be concluded that a small amount of Si (between 4–7 at.%) in Cr coatings is effective in protecting the austenitic stainless steel against oxidation at high temperatures while a high Si content (around 10 at.% or more) makes the coating more brittle and prone to cracking or delamination during oxidation at 800 °C. Further research will be focused on fine microstructure characterization of oxidized CrSi coating to fully understand the oxidation protection mechanism of the coatings with different Si content. Another prospect will be the application of CrSi coatings on different types of substrates, such as thermoelectric materials.

**Author Contributions:** Conceptualization, Z.Z., X.L. and H.D.; methodology, M.G. and X.L.; validation, M.G., Z.Z. and X.L.; formal analysis, M.G. and X.L.; investigation, M.G. and X.L.; resources, M.G.; data curation, M.G. and X.L.; writing—original draft preparation, M.G. and X.L.; writing—review and editing, Z.Z., X.L. and H.D.; visualization, M.G.; supervision, Z.Z., X.L. and H.D.; project administration, Z.Z. and H.D.; funding acquisition, H.D. All authors have read and agreed to the published version of the manuscript.

**Funding:** This research was funded by the EU H2020 Project ‘FAST and Nano-enabled SMART materials, Structure and System for Energy Harvesting’ (FAST-SMART) under grant number 862289 and supported by the Ministry of National Education of the Republic of Turkey.

**Institutional Review Board Statement:** Not applicable.

**Informed Consent Statement:** Not applicable.

**Data Availability Statement:** Not applicable.

**Conflicts of Interest:** The authors declare no conflict of interest.

## References

1. Adzali, N.M.S.; Azhar, N.A.; Che Daud, Z.; Ahmad Zaidi, N.H.; Adnan, S.A. Heat Treatment of SS 316L for Automotive Applications. In *Materials Science Forum*; Trans Tech Publications: Bäch, Switzerland, 2020; pp. 28–33.
2. Baldev, R.; Kamachi Mudali, U.; Vijayalakshmi, M.; Mathew, M.D.; Bhaduri, A.K.; Chellapandi, P.; Venugopal, S.; Sundar, C.S.; Rao, B.P.C.; Venkatraman, B. Development of Stainless Steels in Nuclear Industry: With Emphasis on Sodium Cooled Fast Spectrum Reactors History, Technology and Foresight. *Adv. Mater. Res.* **2013**, *794*, 3–25. [[CrossRef](#)]
3. Harshini, D.; ul Haq, A.; Buddi, T.; Kumar, K.A.; Lakshmi, A.A. Comparative study on mechanical behavior of ASS 316L for low and high temperature applications. *Mater. Today Proc.* **2019**, *19*, 767–771. [[CrossRef](#)]
4. Wu, X.-Y.; Sun, J.-K.; Wang, J.-M.; Jiang, Y.-M.; Li, J. Crevice Corrosion Behaviors Between CFRP and Stainless Steel 316L for Automotive Applications. *Acta Metall. Sin. Engl. Lett.* **2019**, *32*, 1219–1226. [[CrossRef](#)]
5. Lo, K.H.; Shek, C.H.; Lai, J.K.L. Recent developments in stainless steels. *Mater. Sci. Eng. R Rep.* **2009**, *65*, 39–104. [[CrossRef](#)]
6. Wang, W.; Guan, B.; Li, X.; Lu, J.; Ding, J. Corrosion behavior and mechanism of austenitic stainless steels in a new quaternary molten salt for concentrating solar power. *Sol. Energy Mater. Sol. Cells* **2019**, *194*, 36–46. [[CrossRef](#)]
7. Asraff, A.; George, M.V.; Jayamani, K.; Sarath Chandran Nair, S. Evaluation of viscoplastic parameters of an austenitic stainless steel at high temperature. In *Proceedings of Fatigue, Durability and Fracture Mechanics*; Springer: Berlin/Heidelberg, Germany, 2018; pp. 7–28.
8. Swales, F.M. The application of cast austenitic stainless steels in high temperature petrochemical services. In *Proceedings of the 6th World Petroleum Congress, Frankfurt am Mein, Germany, 19–26 June 1963*; OnePetro: Richardson, TX, USA, 1963.
9. Andrei, V.A.; Radulescu, C.; Malinovschi, V.; Marin, A.; Coaca, E.; Mihalache, M.; Mihailescu, C.N.; Dulama, I.D.; Teodorescu, S.; Bucurica, I.A. Aluminum oxide ceramic coatings on 316L austenitic steel obtained by plasma electrolysis oxidation using a pulsed unipolar power supply. *Coatings* **2020**, *10*, 318. [[CrossRef](#)]
10. Kazazi, M.; Haghighi, M.; Yarali, D.; Zaynolabedini, M.H. Improving corrosion resistance of 316L austenitic stainless steel using ZrO<sub>2</sub> sol-gel coating in nitric acid solution. *J. Mater. Eng. Perform.* **2018**, *27*, 1093–1102. [[CrossRef](#)]
11. Batista, J.C.A.; Godoy, C.; Matthews, A. Micro-scale abrasive wear testing of duplex and non-duplex (single-layered) PVD (Ti,Al)N, TiN and Cr-N coatings. *Tribol. Int.* **2002**, *35*, 363–372. [[CrossRef](#)]
12. Huang, S.W.; Ng, M.; Samandi, M.; Brandt, M. Tribological behaviour and microstructure of TiC<sub>x</sub>N<sub>(1-x)</sub> coatings deposited by filtered arc. *Wear* **2002**, *252*, 566–579. [[CrossRef](#)]
13. Marin, E.; Lanzutti, A.; Guzman, L.; Fedrizzi, L. Corrosion protection of AISI 316 stainless steel by ALD alumina/titania nanometric coatings. *J. Coat. Technol. Res.* **2011**, *8*, 655. [[CrossRef](#)]
14. Purushotham, K.P.; Ward, L.P.; Brack, N.; Pigram, P.J.; Evans, P.; Noorman, H.; Manory, R.R. Tribological studies of Zr-implanted PVD TiN coatings deposited on stainless steel substrates. *Wear* **2003**, *254*, 589–596. [[CrossRef](#)]
15. Anwer, Z.; Tufail, M.; Chandio, A.D. Deposition of Aluminide Coatings onto AISI 304L Steel for High Temperature Applications. *Materials* **2022**, *15*, 4184. [[CrossRef](#)]
16. Li, Y.; Zhu, Y.; Ye, Q.; Zhang, S.-Z.; Zhao, J.; He, Y. Effect of Hybrid Surface Treatment Composed of Plasma Nitriding and W-Cr-Ti-Al-N Coating on Tribological Behavior of AISI 316L Steel. *Tribol. Online* **2018**, *13*, 316–319. [[CrossRef](#)]
17. Ye, Q.; Li, Y.; Zhang, M.; Zhang, S.; Bi, Y.; Gao, X.; He, Y. Electrochemical behavior of (Cr, W, Al, Ti, Si) N multilayer coating on nitrated AISI 316L steel in natural seawater. *Ceram. Int.* **2020**, *46*, 22404–22418. [[CrossRef](#)]
18. Huang, J.-H.; Kuo, K.-L.; Yu, G.-P. Oxidation behavior and corrosion resistance of vacuum annealed ZrN-coated stainless steel. *Surf. Coat. Technol.* **2019**, *358*, 308–319. [[CrossRef](#)]
19. Pakseresht, A.H. *Production, Properties, and Applications of High Temperature Coatings*; IGI Global: Hersey, PA, USA, 2018.
20. Tan, K.H.; Rahman, H.A.; Taib, H. Coating layer and influence of transition metal for ferritic stainless steel interconnector solid oxide fuel cell: A review. *Int. J. Hydrog. Energy* **2019**, *44*, 30591–30605. [[CrossRef](#)]
21. Chen, H.; Wang, X.; Zhang, R. Application and development progress of Cr-based surface coating in nuclear fuel elements: II. Current status and shortcomings of performance studies. *Coatings* **2020**, *10*, 835. [[CrossRef](#)]
22. Kashkarov, E.; Sidelev, D.; Syratanov, M.; Tang, C.; Steinbrück, M. Oxidation kinetics of Cr-coated zirconium alloy: Effect of coating thickness and microstructure. *Corros. Sci.* **2020**, *175*, 108883. [[CrossRef](#)]
23. Sharma, R.K.; Das, R.K.; Kumar, S.R. Effect of chromium content on microstructure, mechanical and erosion properties of Fe-Cr-Ti-Mo-C-Si coating. *Surf. Interfaces* **2021**, *22*, 100820. [[CrossRef](#)]
24. Michau, A.; Maury, F.; Schuster, F.; Lomello, F.; Brachet, J.-C.; Rouesne, E.; Le Saux, M.; Boichot, R.; Pons, M. High-temperature oxidation resistance of chromium-based coatings deposited by DLI-MOCVD for enhanced protection of the inner surface of long tubes. *Surf. Coat. Technol.* **2018**, *349*, 1048–1057. [[CrossRef](#)]
25. Lillerud, K.; Kofstad, P. On high temperature oxidation of chromium: I. Oxidation of annealed, thermally etched chromium at 800–1100 C. *J. Electrochem. Soc.* **1980**, *127*, 2397. [[CrossRef](#)]
26. Kofstad, P.; Lillerud, K. On high temperature oxidation of chromium: II. Properties of and the oxidation mechanism of chromium. *J. Electrochem. Soc.* **1980**, *127*, 2410. [[CrossRef](#)]
27. Schütze, M. *Protective Oxide Scales and Their Breakdown*; Wiley: Hoboken, NJ, USA, 1997.
28. Gulbransen, E.A.; Andrew, K.F. Kinetics of the Oxidation of Chromium. *J. Electrochem. Soc.* **1957**, *104*, 334. [[CrossRef](#)]

29. Han, X.; Xue, J.; Peng, S.; Zhang, H. An interesting oxidation phenomenon of Cr coatings on Zry-4 substrates in high temperature steam environment. *Corros. Sci.* **2019**, *156*, 117–124. [[CrossRef](#)]
30. Liu, J.; Steinbrück, M.; Große, M.; Stegmaier, U.; Tang, C.; Yun, D.; Yang, J.; Cui, Y.; Seifert, H.J. Systematic investigations on the coating degradation mechanism during the steam oxidation of Cr-coated Zry-4 at 1200 °C. *Corros. Sci.* **2022**, *202*, 110310. [[CrossRef](#)]
31. Bamba, G.; Wouters, Y.; Galerie, A.; Charlot, F.; Dellali, A. Thermal oxidation kinetics and oxide scale adhesion of Fe–15Cr alloys as a function of their silicon content. *Acta Mater.* **2006**, *54*, 3917–3922. [[CrossRef](#)]
32. Schmitt, T.; Steyer, P.; Fontaine, J.; Mary, N.; Esnouf, C.; O’Sullivan, M.; Sanchette, F. Cathodic arc deposited (Cr, Six) N coatings: From solid solution to nanocomposite structure. *Surf. Coat. Technol.* **2012**, *213*, 117–125. [[CrossRef](#)]
33. Soleimani-Dorcheh, A.; Galetz, M. Oxidation and nitridation behavior of Cr–Si alloys in air at 1473 K. *Oxid. Met.* **2015**, *84*, 73–90. [[CrossRef](#)]
34. Zeng, S.; Tian, J.; Han, X.; Meng, Y.; Zhu, M.; Zhang, H. Oxidation behavior of CrSi coatings on Zry-4 substrates in 1200 °C steam environment. *J. Nucl. Mater.* **2022**, *558*, 153310. [[CrossRef](#)]
35. Mitoraj-Królikowska, M.; Godlewska, E. Oxidation resistance and micromechanical properties of a Ti–46Al–8Nb (at.%) alloy with Cr–Si magnetron-sputtered coatings. *Surf. Coat. Technol.* **2018**, *350*, 732–739. [[CrossRef](#)]
36. He, X.; Zhan, H.; Lin, J.; Liang, G.; Yang, S.; Meng, C.; Ma, X.; Tan, J.; Liu, M. Effect of Si content of CrSi-based coatings on their oxidation resistance in high temperature air. *Ceram. Int.* **2020**, *46*, 11357–11363. [[CrossRef](#)]
37. Protsenko, V.; Danilov, F. Chromium electroplating from trivalent chromium baths as an environmentally friendly alternative to hazardous hexavalent chromium baths: Comparative study on advantages and disadvantages. *Clean Technol. Environ. Policy* **2014**, *16*, 1201–1206. [[CrossRef](#)]
38. Saha, R.; Nandi, R.; Saha, B. Sources and toxicity of hexavalent chromium. *J. Coord. Chem.* **2011**, *64*, 1782–1806. [[CrossRef](#)]
39. Gokhale, A.; Abbaschian, G. The Cr–Si (Chromium–Silicon) system. *J. Phase Equilibria* **1987**, *8*, 474–484. [[CrossRef](#)]
40. Godlewski, J.; Lambertin, M.; Gros, J.; Wadier, J.; Weidinger, H. Raman spectroscopy study of the tetragonal-to-monoclinic transition in zirconium oxide scales and determination of overall oxygen diffusion by nuclear microanalysis of O<sup>18</sup>. In Proceedings of the American Society for Testing and Materials (ASTM) International Symposium on Zirconium in the Nuclear Industry, Kobe, Japan, 5–8 November 1990.
41. Van Uffelen, P.; Pastore, G. *Oxide Fuel Performance Modeling and Simulation*; Elsevier: Amsterdam, The Netherlands, 2020.

**Disclaimer/Publisher’s Note:** The statements, opinions and data contained in all publications are solely those of the individual author(s) and contributor(s) and not of MDPI and/or the editor(s). MDPI and/or the editor(s) disclaim responsibility for any injury to people or property resulting from any ideas, methods, instructions or products referred to in the content.